J|A|C|S
ARTICLES
Published on Web 04/29/2006

Direct Determination of Low-Dimensional Structures: Synchrotron X-ray Scattering on One-Dimensional Charge-Ordered MMX-Chain Complexes

Yusuke Wakabayashi,*,† Atsushi Kobayashi,‡ Hiroshi Sawa,† Hiroyuki Ohsumi,§ Naoshi Ikeda,§,⊥ and Hiroshi Kitagawa‡

Contribution from the Photon Factory, Institute of Materials Structure Science, High Energy Accelerator Research Organization, Tsukuba 305-0801, Japan, Department of Chemistry, Faculty of Science, Kyushu University, Hakozaki, Fukuoka 812-8581, Japan, and Japan Synchrotron Radiation Research Institute (JASRI), Mikazuki, Hyogo 679-5198, Japan

Received January 12, 2006; E-mail: yusuke.wakabayashi@kek.jp

Abstract: A powerful method to determine the hidden structural parameters in functional molecules has been developed. Local valence arrangements that dominate the material properties are sometimes not three-dimensionally ordered. This method that comprises diffuse X-ray scattering and resonant X-ray scattering is suitable in such cases. Using this method, we present clear evidence of the low-dimensional valence arrangement in two halogen-bridged one-dimensional metal complexes, so-called MMX chains. This family allows us to control many physical and structural parameters by chemical substitution of bridging halogen, counterions, or metal ions, and one of our samples carries an unusual metallic phase. It is demonstrated with this complex that the present method makes it possible to have microscopic insight to low-dimensionally ordered systems.

1. Introduction

Recent development of synchrotron-based X-ray diffraction techniques together with modern methods of analysis, such as the maximum entropy method, makes it possible to discuss the electronic states of materials.[1−3] The electronic states often depend on the atomic arrangement of specific small volumes in a unit cell or molecule (hereafter referred to as the local structure). Knowledge of the local structure is essential to understand the functions of biomolecules or materials composed of large molecules, such as hemoglobin, because the local structure often affects their functions significantly. A change in local structure does not necessarily form a three-dimensional (3D) ordering. This means that most of the analyzing methods as well as ordinary structure analysis provide insufficient results to clarify the electronic states in some cases; they are based on the 3D ordering of the atomic arrangement and, therefore, do not give a low-dimensional ordering that produces no Bragg reflections but does produce diffuse X-ray scattering. Despite its importance, the method to observe the local structure has been limited, and therefore, local structures and its low-dimensional ordering have been imagined based on the result of structure analysis. In this study, we present a powerful method of observing local structure by focusing on diffuse X-ray scattering. The samples were halogen-bridged quasi-1D metal complexes. Such complexes are well-known as possible materials for high-performance optical devices due to their huge third-order nonlinear optical susceptibilities,[4] and one of the samples we measured here attracts considerable interest for its high electric conductivity.

Diffuse X-ray scattering directly shows deviation from the averaged 3D structure, and therefore, in principle, one can extract the low-dimensional structure from its intensity distribution. For example, crystals having a 1D structure produce planar diffuse scattering as well as sharp Bragg reflections given by the averaged 3D structure. One possible way to analyze the diffuse scattering is the pair distribution function analysis.[5] It treats Fourier transformation of all scattering intensity and gives some structural information corresponding not only to 3D structures but also to 1D structures. However, for the purpose of clarifying the low-dimensional structure, Bragg intensity serves simply as an enormous background. The direct way to analyze low-dimensional structures is to examine diffuse intensities, though this type of analysis is often very difficult. One of the main causes of this difficulty is the amount of data. One can measure only dozens of intensities of diffuse scattering planes for 1D structure, while usually thousands of Bragg intensities are available for structure analysis. This gives

† High Energy Accelerator Research Organization.
‡ Kyushu University.
§ Japan Synchrotron Radiation Research Institute (JASRI).
⊥ Present address: Department of Physics, Okayama University, Tsushima-naka, Okayama 700-8530, Japan.

(1) Takata, M.; Umeda, B.; Nishibori, E.; Sakata, M.; Saito, Y.; Ohno, M.; Shinohara H. *Nature* **1995**, *377*, 46−49.
(2) Takata, M.; Nishibori, E.; Kato, K.; Sakata, M.; Moritomo, Y. *J. Phys. Soc. Jpn.* **1999**, *68*, 2190−2193.
(3) Sawa, H.; Wakabayashi, Y.; Murata, Y.; Murata, M.; Komatsu, K. *Angew. Chem., Int. Ed.* **2005**, *44*, 1981−1983.
(4) Kishida, H.; Matsuzaki, H.; Okamoto, H.; Manabe, T.; Yamashita, M.; Taguchi, Y.; Tokura, Y. *Nature* **2000**, *405*, 929−932.
(5) Billinge, S. J. L.; Kanatzidis, M. G. *Chem. Commun.* **2004**, *2004*, 749−760.

10.1021/ja060111j CCC: $33.50

insufficient constraint for the structural model to obtain the chain structure. The present method, however, provides strong constraint for the model. The technique is a scattering method combined with spectroscopic techniques and provides scattering amplitudes from specific elements that are useful in estimating the reliability of a structure model. Another difficulty is the lack of a standard process of analysis, while many powerful direct method software programs are available for 3D ordered systems. In the present work, we applied Fourier analysis of diffuse intensity, which provides an image, pair distribution function, of atomic displacements in real space. Using these techniques, the 1D structures of two metal complexes were successfully obtained in section 3. Direct observation of the low-dimensional structure makes it possible to have further detailed insight into the material property, as demonstrated in section 4.

Because of its spatially narrow electron distribution, the 1D chain compounds of σ-electrons are outstanding among various 1D systems. A typical σ-based 1D system is the halogen-bridged mono/binuclear quasi-1D metal complex, the so-called MX/MMX chain, whose unique properties have been extensively studied.[6−10] The fundamental structure of such complexes is based on the coordination bond of metal ions; this robust configuration makes it possible to control their inter- and intrachain interaction parameters by changing the ligand molecules, counterions, metal, and halogen species of the complexes. This tunability makes the MX/MMX chain a good model of 1D electronic systems that has various electronic phases. Using this tunability, some MMX complexes having metallic conductivity have been produced.[11,12] The MMX complexes are classified into two families by their ligands: one is the *pop* family having *pop* = $P_2O_5H_2^{2-}$ as ligands, which is composed of ionic chains and counterions, and the other is the *dta* family (*dta* = dithioacetate) having $C_nH_{2n+1}CS_2^-$ as ligands, which does not have counterions. Only a part of the latter shows the metallic conductivity. However, the source of the conductivity has not yet been determined. This is an important problem because the mechanism of conduction in an MMX system must be a typical conduction mechanism for σ-based 1D system.

The MMX complexes[13,14] have large degrees of freedom within a chain that involves complicated electronic structures; the four types of valence arrangements shown in Figure 1 are widely used to analyze their magnetic, electric, and spectroscopic properties,[11,15−17] although much more complicated arrangements have also been examined theoretically.[18] In a real system, the average-valence (AV), charge-polarization (CP), and charge-density-wave (CDW) phases are confirmed in complexes of the *pop* family,[14,16,19] and the alternate-charge-polarization (ACP) phase is observed in some of the *dta* family.[20] Since all *pop* complexes are insulating while some *dta* complexes are metallic, one expects there is a relationship between the stability of the ACP and conductivity. To examine this idea, it is essential to clarify the low-dimensional electronic structure. Theoretically, the stabilization of ACP in the *dta* family is understood through intrachain transfer and Coulomb and elastic interactions,[15] and interchain interaction is assumed to be weak. This 1D interaction produces a low-dimensional electronic structure, which is reflected in a low-dimensional structure through electron−lattice coupling.

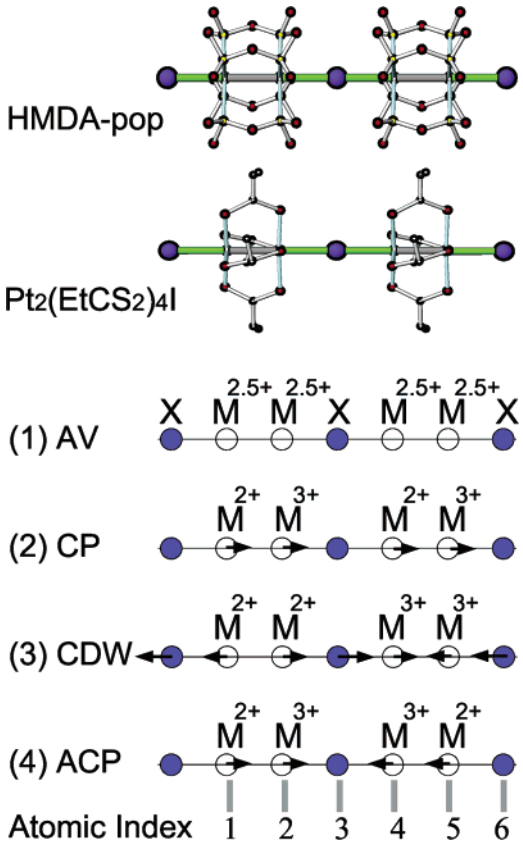

Figure 1. Schematic view of the possible valence arrangement in MMX complex and expected concomitant displacement of atoms; (1) average-valence state, (2) charge-polarization state, (3) charge-density-wave state, and (4) alternate-charge-polarization state. Chain structures of **1** and **3** are shown at the top of the figure.

The samples measured were $[NH_3(CH_2)_6NH_3]_2[Pt_2(pop)_4I]$ (**1**, HMDA-pop), $[(C_2H_5)_2NH_2]_4[Pt_2(pop)_4I]$ (**2**, DEA-pop), and $Pt_2(EtCS_2)_4I$ (Et = C_2H_5, **3**). The complex **1** has the 1D valence arrangement of CDW, while **2** has a CP-type 1D arrangement;[21] these complexes are classified as belonging to the *pop* family. Using these well characterized samples, we successfully established a technique to determine the chain structure. Complex

(6) Okamoto, H.; Mitani, T.; Toriumi, K.; Yamashita, M. *Phys. Rev. Lett.* **1992**, *69*, 2248−2251.
(7) Kuroda, N.; Wakabayashi, Y.; Nishida, M.; Wakabayashi, N.; Yamashita, M.; Matsushita, N. *Phys. Rev. Lett.* **1997**, *79*, 2510−2513.
(8) Sugita, A.; Saito, T.; Kano, H.; Yamashita, M.; Kobayashi, T. *Phys. Rev. Lett.* **2001**, *86*, 2158−2161.
(9) Tomimoto, S.; Saito, S.; Suemoto, T.; Takeda, J.; Kurita, S. *Phys. Rev. B* **2002**, *66*, 155112-1-10.
(10) Baeriswyl, D.; Bishop, A. R. *J. Phys. C: Solid State Phys.* **1988**, *21*, 339−356.
(11) Kitagawa, H.; Onodera, N.; Sonoyama, T.; Yamamoto, M.; Fukawa, T.; Mitani, T.; Seto, M.; Maeda, Y. *J. Am. Chem. Soc.* **1999**, *121*, 10068−10080.
(12) Mitsumi, M.; Murase, T.; Kishida, H.; Yoshinari, T.; Ozawa, Y.; Toriumi, K.; Sonoyama, T.; Kitagawa, H.; Mitani, T. *J. Am. Chem. Soc.* **2001**, *123*, 11179−11192.
(13) Che, C.; Herbstein, F. H.; Schaefer, W. P.; Marsh, R. E.; Gray, H. B. *J. Am. Chem. Soc.* **1983**, *105*, 4604−4607.
(14) Kurmoo, M.; Clark, R. J. H. *Inorg. Chem.* **1985**, *24*, 4420−4425.
(15) Kuwabara, M.; Yonemitsu, K. *J. Mater. Chem.* **2001**, *11*, 2163−2175.
(16) Yamashita, M.; Miya, S.; Kawashima, T.; Manabe, T.; Sonoyama, T.; Kitagawa, H.; Mitani, T. *Synth. Met.* **1999**, *103*, 2164−2165.
(17) Marumoto, K.; Tanaka, H.; Kuroda, S.; Miya, S.; Kawashima, T.; Yamashita, M. *Solid State Communication* **2001**, *120*, 101−106.
(18) Yamamoto, S. *Phys. Rev. B* **2001**, *63*, 125124-1-16.
(19) Yamashita, M.; Toriumi, K. *Inorg. Chim. Acta* **1990**, *178*, 143−149.
(20) Mitsumi, M.; Kitamura, K.; Morinaga, A.; Ozawa, Y.; Kobayashi, M.; Toriumi, K.; Iso, Y.; Kitagawa, H.; Mitani, T. *Angew. Chem., Int. Ed.* **2002**, *41*, 2767−2771.
(21) Matsuzaki, H.; Matsuoka, T.; Kishida, H.; Takizawa, K.; Miyasaka, H.; Sugiura, K.; Yamashita, M.; Okamoto, H. *Phys. Rev. Lett.* **2003**, *90*, 46401-1-4.

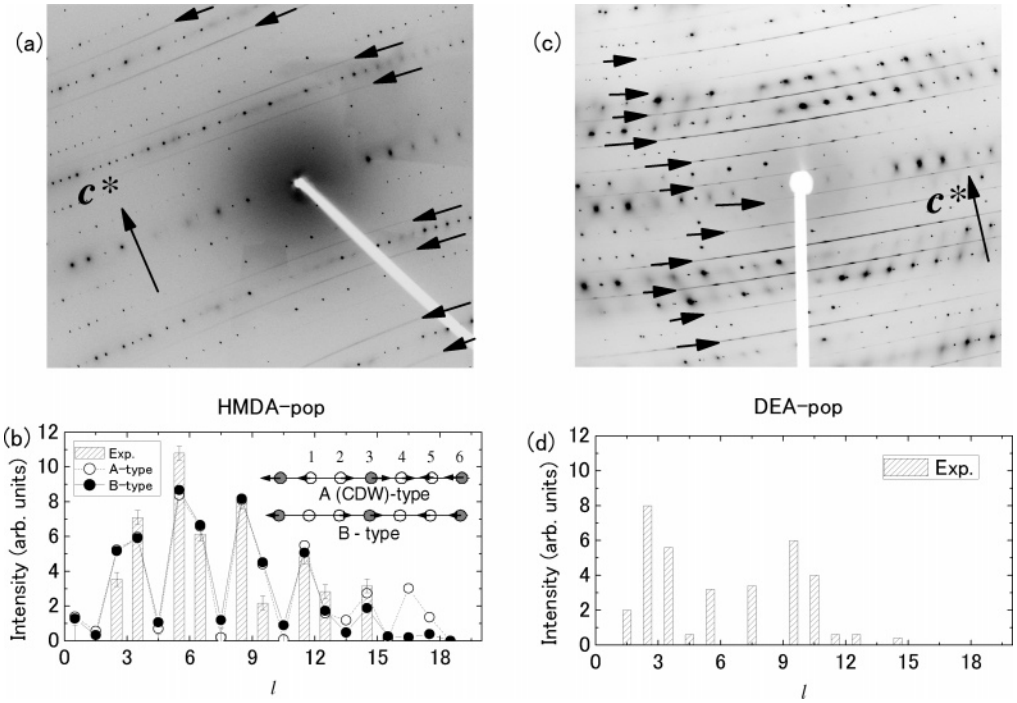

Figure 2. (a) Oscillation photograph of **1** at room temperature. Diffuse streaks characterized by the wave vector $c^*/2$ are clearly observed. (b) Diffuse intensity distribution of **1** on the c^*-axis. Schematic views of the atomic displacement patterns producing good fittings are shown in the inset. (c) Oscillation photograph of **2** at room temperature. (d) Diffuse intensity distribution of **2** on the c^*-axis.

3, which belongs to the *dta* family, is a conductive MMX complex[12] whose electronic structure remains controversial. The structure of the conductive phase is known to be a low-dimensional two-fold structure, and that of the insulating phase is reported to have an ACP-type valence arrangement.[20] The valence arrangement of **3** in the conductive phase was studied by this new method.

2. Experiment

Synchrotron X-ray diffraction measurements were performed at beamlines BL-1A, 1B, and 4C of the Photon Factory, KEK, Japan. These beamlines have bending magnets as their light sources. An X-ray beam is monochromatized by a flat double-crystal Si (111) monochromator and focused on the sample position by a Rh coated bent cylindrical mirror. The spot size at the sample position is 0.5 mm (vertical) × 0.7 mm (horizontal).

BL-1B, which has an imaging-plate Weissenberg camera, was used for sample characterization and for observing the overall features of diffuse scattering distribution. BL-4C has a standard four-circle diffractometer. An ion chamber and a scintillation counter were used as a beam monitor and a signal detector, respectively. BL-1A has both types of diffractometers. A nitrogen gas flow temperature controller was used to cool the sample at all beamlines.

In addition, we conducted diffuse intensity measurements using X-rays having the energies of Pt and I absorption edges. Measurement at the Pt L_{III} absorption edge was made at the Photon Factory BL-4C, and that at the I *K*-edge was made at BL-02B1, SPring-8, Japan. For the former experiments, we used an NaI(Tl) scintillation counter because the NaI(Tl) detector has high sensitivity at Pt L_{III}-edge energy. For the latter experiments, we used a YAP(Ce) scintillation counter because the sensitivity of the NaI(Tl) scintillator has a large energy dependence at the I absorption edge.

Single-crystal samples of **1**, **2**, and **3** were prepared following the method previously reported.[12,13,22] The typical sizes of the samples used were the following: **1**, 600 μm × 30 μm × 30 μm; **2**, 2 mm × 1 mm × 1 mm; and **3**, 300 μm × 50 μm × 5 μm. The typical full width at half-maximum (fwhm) of the rocking curve of an as grown sample was 0.04°. This value was enlarged by several hours of irradiation by synchrotron radiation. To avoid degradation of the data due to radiation damage, the samples were replaced after several hours of irradiation.

3. Results and Analysis

3.1. *pop* Complexes. Oscillation photographs and the diffuse intensity distribution on the c^*-axis, which corresponds to the chain axis, of **1** and **2** are shown in Figure 2. Both samples show diffuse scattering characterized by the wave vector $c^*/2$, indicating that the periodicity of each chain is doubled. Note that their diffuse intensity distributions differ from each other.

Performing a Fourier transformation of these intensity distributions produces the pair distribution function in real space[23] shown in the right-hand side of Figure 3. This operation is almost the same as that used in the Patterson method, i.e., the Fourier transformation of Bragg intensity, which is used for ordinary structure analysis. The difference between the Fourier transformation of Bragg intensity and that of diffuse intensity is the correlation provided: the former gives the pair distribution function of averaged electron density, while the latter provides that of the deviation of the electron density distribution from the averaged distribution. Here, we present what is observed by diffuse scattering using a simple model of an MMX chain having 1D ACP ordering. As shown in the left-hand side of Figure 3, an ACP chain is expected to have displacements of metal ions. The electron density of such a chain is represented by the red line in the left-hand side of this figure. However, in an average structure obtained by ordinary structure analysis, the electron density splits into two sites with occupancy of one-

(22) Takizawa, K.; Ishii, T.; Miyasaka, H.; Matsuzaka, H.; Yamashita, M.; Kawashima, T.; Matsuzaki, H.; Kishida, H.; Okamoto, H. *Mol. Cryst. Liq. Cryst.* **2002**, *376*, 159−164.
(23) Guinier, A. *X-ray diffraction*; W. H. Freeman and Co.: San Francisco, CA, 1963.

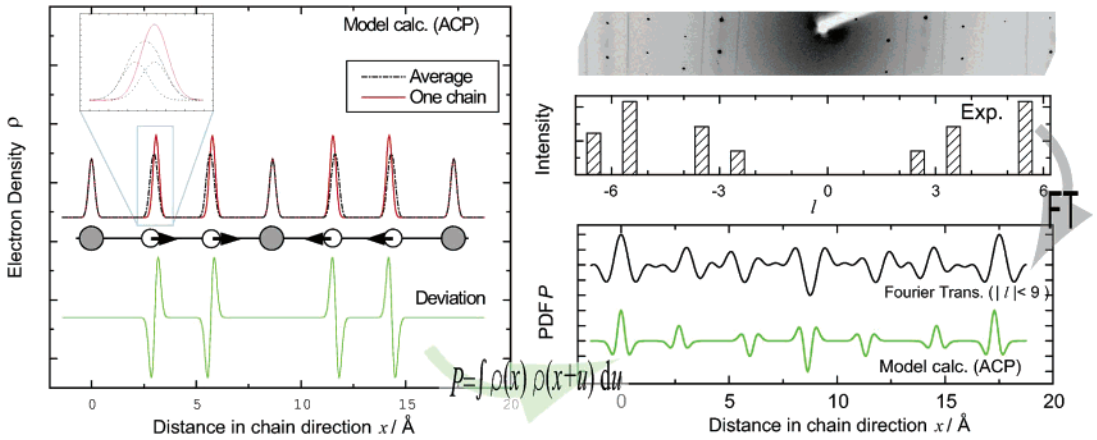

Figure 3. A simple model of the electron density distribution along a 1D ACP chain. The black dash−dotted line shows the averaged electron density, the red line shows the electron density of one chain, and the green line shows the difference between them. (Inset) Magnified view of the electron density around a metal site. The metal position in a chain is fixed while that of the average structure splits into two sites with an occupancy of one-half.

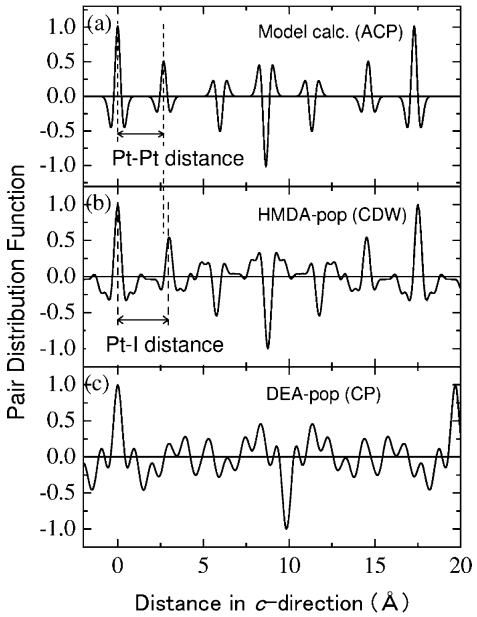

Figure 4. Pair distribution function of (a) 1D ACP model, (b) **1**, and (c) **2**.

half because the position of the metal ion does not have 3D ordering. This situation is shown by the black dash−dotted line and dashed lines in this figure. Therefore, the obtained deviation of the electron density from the average is represented by the green line in the figure; the shape of the first derivative of Gaussian indicates the atomic displacement.

The distribution function of this deviation is shown in the right-hand side of Figure 3 with the green line; the same one is shown in Figure 4a. A pair distribution function having the shape of the second derivative of Gaussian, which is shown in the region of ±2 Å in the figures, is characteristic of atomic displacement along the *c*-axis.[24] Furthermore, the ACP model calculation shows a sharp positive peak at the Pt−Pt distance, indicating that the two neighboring Pt atoms move in the same direction from the average position.

The pair distribution function for **1** is shown in Figure 4b. The distribution function in the region of ±2 Å is very similar to the calculation for the 1D ACP model, indicating that **1** contains atomic displacements. In contrast, the distribution function for **2** shown in Figure 4c does not show this type of feature, indicating that **2** does not contain the alternation of atomic displacement along the chain axis. The observed lack of atomic displacement having 2*c* periodicity in **2** coincides with the expected distortion for the CP phase shown in Figure 1. The diffuse scattering of **2** shows the existence of an amplitude modulation[23] such as alternation of occupancy. In clarifying the electronic state, this kind of scattering has no importance because the valence arrangement is reflected in displacements.

Next, we examine the pair distribution function of **1** (Figure 4b). A large negative correlation is found at position 8.753 Å, the *c*-lattice constant, indicating that the displacement vector of an atom is antiparallel to that of the atom at 8.753 Å away from the first atom; this corresponds to the two-fold structure. A positive correlation at 2.99 Å is also found, indicating that the displacement vectors of two atoms whose distance is 2.99 Å have the same direction. This distance is close to Pt−I distance 2.96 Å and far from Pt−Pt distance 2.84 Å. Therefore, neighboring Pt and I ions move in the same direction from the average position in this complex; the slight difference of 0.03 Å is attributable to the cutoff error of the Fourier transform. This displacement pattern coincides with the CDW-type atomic displacement shown in Figure 1.

A quantitative analysis of the diffuse intensity distribution was made to obtain the chain structure. As mentioned above, this diffuse scattering is caused by atomic displacement of Pt and I along the *c*-axis. The diffuse scattering intensity at the scattering vector ($\xi\eta\zeta$) is therefore written as follows:

$$I(\xi\eta\zeta) = L(2\zeta)N_xN_y\left|\sum_j f_j \exp[i\vec{Q}\cdot(\vec{R}_j + \vec{\delta}_j)]\right|^2 \qquad (1)$$

where N_x and N_y are the number of chains in the *a*- and *b*-directions, $L(\zeta)$ is the Laue function corresponding to the *c**-direction, $\vec{Q}$ is the scattering vector, and f_j, $\vec{R}_j$, and $\vec{\delta}_j$ are the scattering factor, average position, and displacement of the *j*th atom, respectively. The summation includes consecutive Pt−Pt−I−Pt−Pt−I units in order to take into account the two-fold structure. They are denoted by indices $j = 1-6$, as shown in Figure 1. We treat $\vec{R}_j$ and $\vec{\delta}_j$ as scalars because the atomic displacements are constrained in the chain direction. The right-hand side of this equation is independent of the parameters ξ

(24) Wakabayashi, Y.; Wakabayashi, N.; Yamashita, M.; Manabe, T.; Matsushita, N. *J. Phys. Soc. Jpn.* **1999**, *68*, 3948−3952.

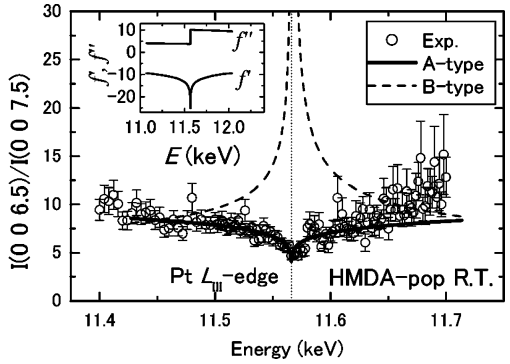

Figure 5. Incident energy dependence of the ratio $I(0\ 0\ 6.5)/I(0\ 0\ 7.5)$ of **1**. The solid and dashed lines denote the calculated values for A-type and B-type structures, respectively. (Inset) Energy dependence of the atomic form factor of Pt:[25] $f_{Pt} = f_0 + f' + if''$, where f_0 is the normal part of the form factor of Pt.

and η, indicating that the intensity distribution forms a plane. Diffuse scattering was observed only at ζ = odd/2, as shown in Figure 2a. This fact and eq 1 show the relationship $\delta_l = -\delta_{l+3}$. For odd values of l, the intensity at $00(l/2)$ is written as

$$I\left(00\frac{l}{2}\right) \propto \left|\sum_j f_j \exp[2\pi i l(R_j + \delta_j)]\right|^2 \quad (2)$$

$$\propto |f_{Pt}(e^{2\pi i l D}\sin(2\pi l\delta_1) - e^{-2\pi i l D}\sin(2\pi l\delta_2)) + f_I \sin(2\pi l\delta_3)|^2, \quad (3)$$

where D denotes the Pt−I distance in the unit of $2c$ (for **1**, $D = 0.169$), and f_{Pt} and f_I are the form factors of Pt and I, respectively. The atomic displacement parameters $\delta_{1,2,3}$ were estimated by the least-squares fitting technique using this equation. CDW-type atomic displacements, (A) $\delta_1 = -\delta_2 = -0.04$ Å and $\delta_3 = 0.2$ Å, give good agreement between the calculated and measured intensity distributions, as shown in Figure 2b. This type of structure is consistent with the constraint obtained by the pair distribution function, which shows that neighboring Pt and I ions move in the same direction from the average position. This constraint allows another structure, case B shown in the inset of Figure 2b, although this structure is physically implausible. A least-squares analysis gives the displacement parameters of (B)$\delta_1 = -0.02$ Å, $\delta_2 = 0.2$ Å, and $\delta_3 = 0.2$ Å, and the calculated intensity distribution is shown in the same figure. Here, we present an elegant method of excluding the B-type structure, while one can exclude it by an inelegant method, i.e., making a careful analysis of the pair distribution function regarding out-of-chain components. Our method excludes wrong structures by qualitative analysis and gives clearer results for superstructures than those by quantitative analyses, such as those based on the R factor.

Although the calculated intensity distributions on the c*-axis for the two types of structures are very similar, the (00ζ) scattering amplitudes from Pt for the two structures are different. The scattering amplitude from Pt atoms is reflected in the energy dependence of the scattered intensity around the Pt absorption edge because, as shown in the inset of Figure 5, the value of f_{Pt} changes keenly at the edge, while the atomic form factors of other elements have little energy dependence at the edge. In practice, an energy spectrum of scattered intensity is also strongly affected by the energy dependence of the absorption coefficient. To avoid this effect, the ratio $I(0\ 0\ 6.5)/I(0\ 0\ 7.5)$ is used for this analysis. The ratio around the Pt L_{III} absorption edge is shown in Figure 5. This ratio decreases clearly at the absorption edge energy. The solid and dashed lines show the calculated intensity ratio regarding A-type and B-type structures, respectively. The calculated ratio of the A-type structure shows good agreement with our experimental results, while that of the B-type structure is completely different from the observed value.

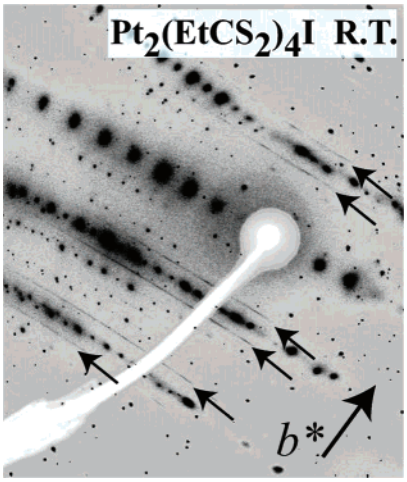

Figure 6. Oscillation photograph of **3** at room temperature. Diffuse streaks characterized by the wave vector b*/2 are clearly observed.

Based on these results, we confirmed that the combined use of the pair distribution function and the energy spectra allows us to observe CDW-type atomic displacement. It should be emphasized that this is the first observation of a long-range-ordered 1D CDW in an MMX system. Although Raman scattering[21] gives two kinds of Pt−Pt stretching mode frequencies, there is no clue of the low-dimensional long-range ordering. Only the analysis of diffuse scattering intensity gives direct evidence of the low-dimensional ordering.

3.2. Valence Arrangement in $Pt_2(EtCS_2)_4I$ (3). An oscillation photograph of **3** is shown in Figure 6. Diffuse scattering characterized by the wave vector b*/2, which corresponds to a two-fold structure within a chain, is clearly observed, as reported in ref 12. The intensity distribution along the a*-direction lacks structure within a Brillouin zone, indicating no spatial correlation along the a-axis. The observed diffuse scattering intensity distribution along the b*-axis at room temperature is shown in Figure 7. The width in the b*-axis shows that the correlation length within a chain is greater than 500 Å. This figure shows the $(0\ k\ 0)$ intensity within the region of $4.5 \le k \le 16.5$. Intense scattering was observed at $k = 3n \pm 0.5$. The intensity distribution is very similar to that of **1**, and the obtained pair distribution function (not shown) indicates the existence of atomic displacements.

The atomic displacement parameters $\delta_{1,2,3}$ were estimated by least-squares fitting using eq 3 with cyclic cell transformation. Two sets of δ's again produce good fittings: (A) $\delta_1 = -0.02$ Å, $\delta_2 = 0.02$ Å, and $\delta_3 = 0.23$ Å (CDW-type structure); and (B) $\delta_1 = 0.00$ Å, $\delta_2 = 0.21$ Å, and $\delta_3 = 0.21$ Å. The energy spectra of the diffuse intensity shown in Figure 8 indicate that the former structure is realized. Figure 8a shows the ratio of the diffuse intensity at (0 6.5 0) to that at (0 7.5 0) around the Pt L_{III} absorption edge as well as the calculated spectrum for the A-type (CDW-type) structure. Furthermore, a similar experi-

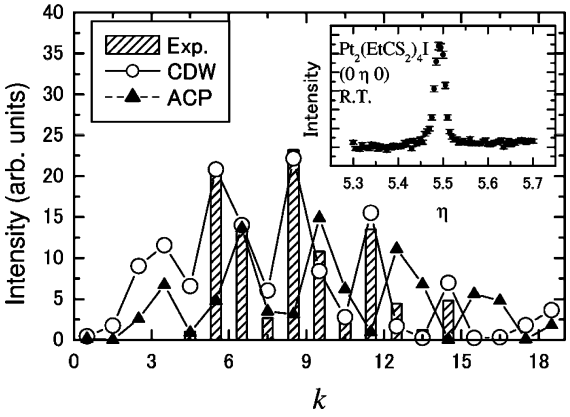

Figure 7. Diffuse scattering intensity distribution along the *b**-axis at room temperature. The calculated intensities of CDW- and ACP-type structures are also plotted. (Inset) Diffuse intensity distribution around (0,5.5,0).

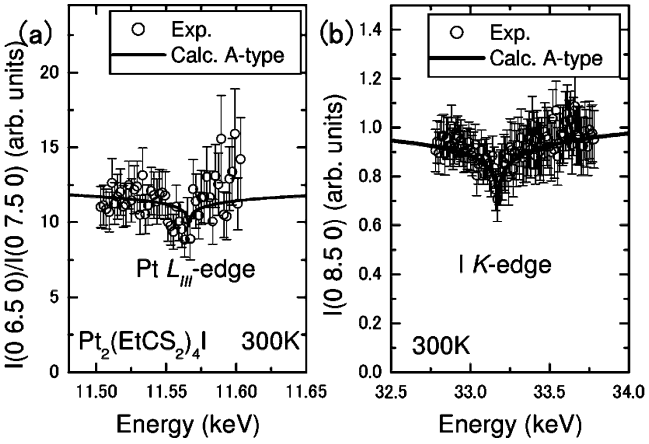

Figure 8. Incident X-ray energy dependence of **3**. (a) Pt L_{III}-edge; (b) I *K*-edge.

ment around the I *K*-absorption edge at (0 8.5 0) was also carried out. In this case, the energy of the X-ray is so high that no distinctive absorption was observed. For this reason, no absorption correction was made on the I *K*-edge data; we corrected only the energy dependence of the detector efficiency using a linear function. The results, which also support the occurrence of CDW in the conductive phase of **3**, are shown in Figure 8b.

The diffuse intensity distribution and energy spectra at 180 K show that the in-chain valence arrangement at 180 K is identical to that at room temperature.

4. Discussion

4.1. Observed Low-Dimensional Structure of 3 and Low-Temperature 3D Structure. The chain structure of **3** was found to be CDW while the 3D-ordered low-temperature structure is the ACP-type structure.[20] Without our analysis, one might expect that the chain structure in high-temperature low-dimensional phase is the same as that of the low-temperature 3D ordering phase. Our results clearly show the lack of the validity of this expectation. For reference, calculated intensity distributions on the *b**-axis for both ACP-and CDW-type structures are presented in Figure 7; the former is completely different from the measured one. This clearly shows that the charge-ordering structure in the conductive phase is different from that reported for the low-temperature insulating phase. This result indicates the importance of the analysis of diffuse scattering; even in a compound that has a 3D ordered low-temperature phase, the chain structure in the 3D ordered structure may differ from the low-dimensional structure.

In this compound, the dimensionality of the superstructure is 2D above 250 K, 1D around 200 K, and 3D below 130 K.[12] This unusual dimensionality is not surprising in light of our findings. The ground state of this system is ACP, and CDW is stable at high temperatures. The 2D correlation of CDW is broken by ACP fluctuation as the sample temperature decreases from room temperature. Finally, 3D ordering of ACP grows to be long-range. Since metallic conductivity or thermoelectric power are reported only in the 2D phase,[12] the metallic behavior was found to have a direct relationship with the 2D-CDW.

4.2. Origin of the 2D-CDW. We *observed* the low-dimensional structure while previous studies *discussed* it based on structure analysis and other properties.[12,20] Now we can make further detailed insights into the material. In this section, we discuss the origin of the 2D-CDW, which is found to be a key factor of the conductivity in **3**. In previous studies, the CDW state was reported for the *pop* family by Raman scattering,[16,17] and it is confirmed by the present work. For the *dta* family, this state has not yet been reported, while the ACP state has been clearly observed in **3**, $BuCS_2$, and $PenCS_2$ complexes (Bu = C_4H_9 and Pen = C_5H_{11}) at low temperatures.[20,26] The CDW was first observed in **3**, and our preliminary measurements show that the $MeCS_2$ complex (Me = CH_3) also has a CDW state; it appears that small ligands prefer the CDW state. In this section, we explain this tendency using the one-band model presented by Kuwabara and Yonemitsu[15] first. Later, the dimensionality of the CDW is microscopically inspected.

The one-band model takes into account the inter-binuclear transfer t_{MM}, the transfer integral between two metals through the bridging halogen t_{MXM} that depends on the M−X−M distance, the electron−lattice coupling constant β, the elastic constants K_{MX} and K_{MXM} regarding M−X and M−X−M lengths, and on-site/long-range Coulomb energies. CDW is stabilized by t_{MM} through the second-order perturbation process and electron−lattice coupling β, while ACP is stabilized by β and the alternation of t_{MXM} caused by alternation of the M−X−M distance. In other words, small K_{MXM} that produces large alternation of the M−X−M distance is required to stabilize the ACP state. In *pop* compounds, counterions block changes in the M−X−M distance, as shown in Figure 9a. This steric hindrance gives a large value of K_{MXM} and results in the absence of ACP in *pop* compounds. For the *dta* family, in ref 15, small K_{MXM} is adopted, which stabilizes ACP significantly, because it has no counterions. As theoretically expected, the structural analysis of the $BuCS_2$ complex clearly shows an ACP state;[20] however, the present results show that $MeCS_2$ and $EtCS_2$ complexes have CDW states.

Our experimental results for the *dta* family show that smaller ligand molecules tend to stabilize the CDW state. Figure 9b shows the structures of $Pt_2(EtCS_2)_4I$ (**3**); the structures of $Pt_2(MeCS_2)_4I$ and $Pt_2(BuCS_2)_4I$ are very similar to that of **3**. The ligand−ligand distance for $MeCS_2$, $EtCS_2$, and $BuCS_2$ complexes are 3.8, 4.4, and 5.2 Å, respectively. The counterion−ligand distance in **1**, shown in Figure 9a, is 3.8 Å and is

(25) Sasaki, S. *KEK Rep.* **1989**, *88*−*14*.
(26) Tanaka, H.; Kuroda, S.; Yamashita, T.; Mitsumi, M.; Toriumi, K. *J. Phys. Soc. Jpn.* **2003**, *72*, 2169−2172.

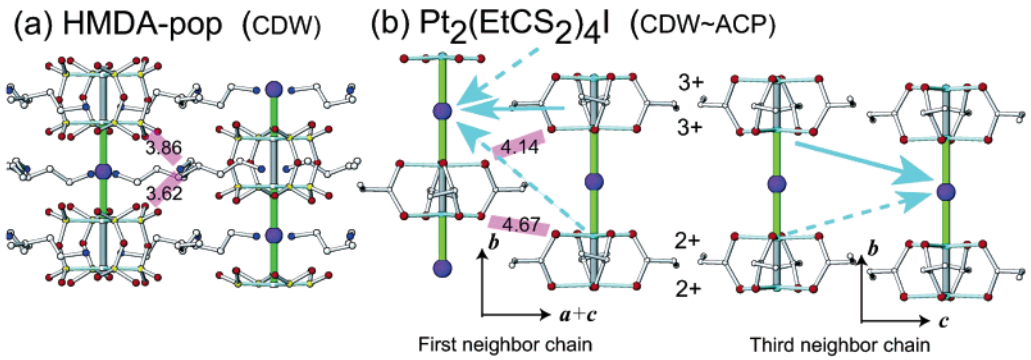

Figure 9. Structure of (a) HMDA-pop (**1**) and (b) $Pt_2(EtCS_2)_4I$ (**3**). Counterions in **1** (ligands of the nearest neighbor chain in **3**) block the displacement of metal dimer units because the distances shown by the pink bars are small. Interchain interactions in **3** shown by blue arrows (Pt^{3+}−I) and blue dashed arrows (Pt^{2+}−I) give the two-dimensionality of the CDW.

comparable to the ligand−ligand distance in $Pt_2(MeCS_2)_4I$. In a naive argument, this produces a comparable value of K_{MXM}. The ligand−ligand distance increases with the increasing size of ligand molecule; this results in a decrease in K_{MXM}. Since small K_{MXM} stabilizes the ACP state, we conclude that K_{MXM} for $MeCS_2$ is not small enough to stabilize the ACP state and that the $EtCS_2$ complex is very close to the ACP−CDW phase boundary.

The 2D-CDW observed at room temperature is given by the interchain interaction between the third-neighbor chains. Here, the interchain distances for the first, second, and third neighbors are 8.32, 8.72, and 9.28 Å, respectively. At room temperature, diffuse scattering spread along the a^* direction was observed, indicating that the phase of the CDW is coherent in a $b-c$ plane, which is shown in the right-hand portion of Figure 9b. The CDW was found to be aligned in-phase within this plane based on the finite intensity on the (0 k 0) axis. The blue arrows (Pt^{3+}−I) and blue dashed arrows (Pt^{2+}−I) in Figure 9b show the interchain interaction among the Pt and I ions. The structural relationship between the second-neighbor chains (not shown) is very similar to that between the first neighbors, while it is different from that between the third neighbors. As can be seen in the figure, the b-direction component of the force on the iodine caused by the first (and second) neighbor chain is almost canceled while that caused by the third neighbor chain remains. If the interaction is attractive and the force given by 3+ is stronger than that given by 2+, which is the case for the Coulomb interaction, the iodine ion shown in the rightmost chain in this figure will be attracted upward, and the valence of the ions of the upper Pt dimer in this chain would become 3+ by β. This is the mechanism of 2D-CDW formation.

5. Conclusion

We established a technique for clarifying the low-dimensional structure, which reflects the valence arrangement. Using this technique, the one-dimensional long-range order of CDW in the MMX system was observed in **1** for the first time. The conductive phase of **3** was also examined by this technique, which showed that **3** has a CDW structure while the structure at 48 K,[20] where it is in an insulating phase, is ACP. We conclude that the CDW state in $MeCS_2$ and $EtCS_2$ complexes is stabilized by the large K_{MXM} caused by the short interchain distance. We also discussed the origin of the 2D-CDW that is required for the large conductivity in **3**. Note that the clarification of the low-dimensional structure allows us to discuss the microscopic mechanism.

Acknowledgment. This work was supported by a Grant-in-Aid for Creative Scientific Research (13NP0201) from the Ministry of Education, Culture, Sports, Science and Technology of Japan.

JA060111J